Original Research

Inhibition of cGAS Reduces Brain Injury and Facilitates Neurological Recovery via the STING-Mediated Signaling Pathway After Germinal Matrix Hemorrhage in Neonatal Mice

Yiheng Wang¹, Xuhui Yin¹, Xiaoli Zhang¹, Xixiao Zhu¹, Yiting Luo¹, Bing-Qiao Zhao^{1,2,*}

Academic Editors: Cenglin Xu and Bettina Platt

Submitted: 26 March 2025 Revised: 5 June 2025 Accepted: 24 June 2025 Published: 22 August 2025

Abstract

Background: Germinal matrix hemorrhage (GMH) is a common complication of premature infants with lifelong neurological consequences. Inflammation-mediated blood-brain barrier (BBB) disruption has been implicated as a main mechanism of secondary brain injury after GMH. The cyclic guanosine monophosphate-adenosine monophosphate synthase (cGAS)-stimulator of interferon genes (STING) pathway plays a crucial role in inflammation, yet its involvement in GMH pathophysiology remains unclear. **Methods**: Collagenase was injected into the right germinal matrix of postnatal day 5 (P5) mouse pups to induce GMH. Either RU.521, or RU.521 combined with a STING agonist SR-717 was administered to the mice after GMH. The number of microglia, proinflammatory cytokines, microglial polarization, BBB permeability, demyelination, and axon degeneration were analyzed by immunofluorescence staining, western blotting, and quantitative real-time PCR. Neurobehavioral functions were evaluated using novel object recognition, Y-maze, and rotarod tests. Results: After induction of GMH, cGAS and STING were upregulated in the peri-hematomal area with a peak at 24 h, and they were mainly expressed in microglia. RU.521 treatment decreased the number of microglia, proinflammatory cytokines and microglial polarization, preserved BBB integrity, and decreased its permeability after GMH. Moreover, RU.521 decreased GMH-mediated upregulation of STING, phosphorylated TANK-binding kinase 1 (phospho-TBK1), phosphorylated interferon regulatory factor 3 (phospho-IRF3), and interferon- β (IFN- β), diminished demyelination, axon degeneration, and neurological deficits. The STING agonist SR-717 blunted RU.521-induced downregulation of phospho-TBK1, phospho-IRF3 and IFN- β and blocked RU.521-mediated inhibition of inflammation, protected against BBB breakdown, white matter lesions, and neurological dysfunction after GMH. Conclusions: Inhibition of cGAS improved white matter lesions and neurological dysfunction by modulating the microglial polarization towards decreased neuroinflammation and maintaining BBB integrity through STING-mediated type I IFN- β production. Thus, cGAS may be a potential therapeutic target for the treatment of GMH.

Keywords: germinal matrix hemorrhage; neuroinflammation; blood-brain barrier disruption; white matter lesions; cGAS; STING/p-TBK1/p-IRF3/IFN- β signaling pathway

1. Introduction

Germinal matrix hemorrhage (GMH) is a devastating disease that predominantly affects preterm and low-birth-weight infants [1]. It is defined as bleeding in the germinal matrix, due to the rupture of blood vessels in the fragile capillary network [2]. GMH frequently progresses to intraventricular hemorrhage, resulting in posthemorrhagic hydrocephalus and periventricular leukomalacia [3,4]. GMH can also increase brain injury to the white matter through inflammation, blood-brain barrier (BBB) disruption, microglial activation, astrogliosis, demyelination, and axon degeneration [5,6]. Despite extensive efforts, currently there are no effective therapies for GMH.

Emerging evidence has highlighted the accumulation of fragmented double-stranded DNA (dsDNA) in brain in-

juries, serving as a critical initiator of neuroinflammation [7]. Cyclic GMP-AMP synthase (cGAS) is a crucial cytoplasmic DNA sensor that detects and binds to both endogenous and exogenous dsDNA, and then converts guanosine triphosphate (GTP) and adenosine triphosphate (ATP) into 2'3' cyclic GMP-AMP (cGAMP), a potent endogenous agonist of stimulator of interferon genes (STING) [8]. The activation of STING leads to the production of type I interferons and inflammatory cytokines, facilitated by TRAF family member-associated NF-κB activator (TANK)-binding kinase 1 (TBK1)-mediated phosphorylation of interferon regulatory factor 3 (IRF3) [9]. Therefore, inhibition of cGAS signaling is likely to be a critical approach to mitigate inflammation and its associated pathology. We previously reported that cGAS is highly expressed in microglia [10], which are resident macrophages of the brain and play im-

¹Institute of Neuroscience and Third Affiliated Hospital, Zhengzhou University, 450052 Zhengzhou, Henan, China

²State Key Laboratory of Medical Neurobiology and MOE Frontiers Center for Brain Science, Institutes of Brain Science, Fudan University, 200032 Shanghai, China

^{*}Correspondence: bingqiaoz@fudan.edu.cn (Bing-Qiao Zhao)

portant roles in pathological immune responses in the brain [11]. Accumulating data indicate that cGAS signaling is markedly increased in brain injuries [12,13], and STING antagonist plays a significant role in the pathogenesis of CNS injury [14]. However, the role of cGAS-mediated signaling activation in GMH remains unclear. RU.521, a potent and selective inhibitor of cGAS, has been reported to block the activation of cGAS-STING signaling pathway by targeting the catalytic pocket of cGAS and inhibiting its binding to dsDNA [15]. Recently, RU.521 has been widely used to explore the mechanisms of cGAS in intrinsic immunity, inflammatory response and autoimmune diseases [16].

In this study, we employed a neonatal mouse model of GMH to investigate the involvement of cGAS-STING pathways in the pathology of GMH. We showed that the cGAS inhibitor RU.521 effectively reduced white matter lesions in the corpus callosum and improved neurological deficits by regulating GMH-triggered inflammatory response and BBB disruption. Our data suggest that this effect may occur through STING-mediated production of type I interferons.

2. Materials and Methods

2.1 Animal GMH Model

All animal experiments were approved by the Animal Ethics Committee of the Third Affiliated Hospital of Zhengzhou University. Postnatal day 5 (P5) C57BL/6 mice were used in this experiment. Mice were maintained at a constant ambient humidity and temperature under a 12hour light/dark cycle with ad libitum access to food and water. The construction of the GMH model using collagenase was performed as previously described [17]. P5 mice were anesthetized with 2% isoflurane (R510-22-10, RWD Life Science, Shenzhen, Guangdong, China) on a brain stereotaxic apparatus, and 0.15 U collagenase VII-S (2399, Sigma-Aldrich, St. Louis, MO, USA) dissolved in 1 μL saline was injected into the right subventricular germinal matrix (AP -2 mm, ML -1 mm, and DV +2 mm, using Bregma as reference) using a 28G needle (7803-2, Hamilton, Reno, MA, USA) and a 25 µL Hamilton syringe connected to a syringe pump (KD Scientific Syringe Pump Company, United States). A heating pad (21100-800, Ugo Basile, Gemonio, VA, Italy) was used to keep the body temperature at 37 \pm 0.5 °C throughout the entire surgical procedure. After GMH induction, mice were administered intraperitoneally with RU.521 (5 mg/kg, HY-114180, MedChemExpress, Monmouth Junction, NJ, USA) or vehicle (10% DMSO (HY-Y0320C, MedChemExpress), 40% PEG300 (HY-Y0873, MedChemExpress), 5% Tween-80 (HY-Y1891, MedChemExpress), and 45% saline) at 1 h after GMH [18]. SR-717 (30 mg/kg, HY-131454, MedChem-Express) or vehicle (50% PEG300 and 50% saline) was injected intraperitoneally immediately after GMH [19].

2.2 Experimental Design and Groups

In this study, both male and female pups were randomly assigned to either sham or GMH group. A total of 148 mice were used. At 24 h, 72 h, 7 days or 28 days after GMH, mice were euthanized by over dose of isoflurane and brains were removed and used for quantitative polymerase chain reaction (qPCR), western blot and immunofluorescence.

Experiment 1. To determine the expression and distribution of cGAS and STING after GMH, mice (n = 20, 5/group) were randomly divided into four groups: sham, GMH 24 h, GMH 72 h, and GMH 7 days. The brain tissues were harvested for western blot analysis. For immunohistochemical quantification of cGAS and STING, 18 mice (n = 6/group) from groups of sham, GMH 24 h, and GMH 72 h were used.

Experiment 2. To explore the effects of RU.521 on inflammation, BBB damage, white matter lesions, and neurological deficits, 66 mice were randomly divided into three groups: sham group, GMH + vehicle group, and GMH + RU.521 group. For qPCR analysis of inflammatory cytokines, 15 mice (n = 5/group) were used. Neurological function was tested on 28 days after GMH (n = 30, 10/group). Additionally, immunofluorescence staining (n = 18, 6/group) and western blotting (n = 15, 5/group) were carried out at 24 h and 28 days after GMH.

Experiment 3. To investigate whether the STING agonist SR-717 could reverse the effects of RU.521 on GMH-induced damage, 44 mice were randomly divided into the GMH + RU.521 + vehicle and GMH + RU.521 + SR-717 groups. Neurological function was tested on 28 days after GMH (n = 20, 10/group). Brain samples were collected for western blot analysis (n = 10, 5/group) and immunofluorescence staining (n = 12, 6/group) at 24 h and 28 days after GMH. Another set of mice were used for qPCR analysis (n = 10, 5/group) at 24 h after GMH.

2.3 Quantitative Real-Time Polymerase Chain Reaction (qPCR)

According to the manufacturer's instructions, total RNA was extracted from brain tissue using the Total RNA Kit (DP419, TIANGEN, Beijing, China). thesis of cDNA was conducted using PrimeScripTM RT Master Mix kit (RR036, TaKaRa, Kyoto, Japan), and qPCR was performed in a LightCycler® 96 gradient machine (Roche, Basel, Switzerland) using PowerUpTM SYBRTM Green premix kit (A25742, Thermo Scientific, Waltham, MA, USA). Relative amount of expression changes in gene levels were calculated using the $2^{-\Delta\Delta CT}$ method [20,21]. Primers used were as follows: GAPDH forward 5'-AGGTCATCCCAGAGCTGAACG-3', reverse 5'-CACCCTGTTGCTGTAGCCGTAT-3', IFN-β forward 5'-GCACTGGGTGGAATGAGACTATTG-3', reverse 5'-TTCTGAGGCATCAACTGACAGGTC -3', $IL-1\beta$ forward 5'-TGAAATGCCACCTTTTGACAG-3',



reverse 5'-CCACAGCCACAATGAGTGATAC-3', IL-6 forward 5'-CTGCAAGAGACTTCCATCCAG-3', verse 5'-AGTGGTATAGACAGGTCTGTTGG-3', TNF-α forward 5'-CCTGTAGCCCACGTCGTAG-3', 5'-GGGAGTAGACAAGGTACAACCC-3', iNOS 5'-GGCACAGGGTCATCATCAAA-3', reverse 5'-TCAGGTCACTTTGGTAGGATTT-3', CD86 forward 5'-GTAGAGTCCAGTTGTTCCTGTC-3', reverse 5'-TGGTTCTGTACGAGCACTATTT-3', Arginase-1 (Arg-1) forward 5'-GTCCCTAATGACAGCTCCTTTC-3', reverse 5'-CCACACTGACTCTTCCATTCTT-3', CD206 forward 5'-GTGGTCCTCCTGATTGTGATAG-3', reverse 5'-CACTTGTTCCTG GACTCAGATTA-3'.

2.4 Western Blot Analysis

For western blot analysis, brain tissues were dissected from the peri-hematomal area (within 1 mm from the edge of the hematoma) as previously described [22]. RIPA lysis buffer containing protease and phosphatase inhibitors (GRF103, Epizyme, Shanghai, China) was used to extract proteins from brain tissue. Proteins were equally loaded, separated using SDS-polyacrylamide electrophoresis and transferred onto the polyvinylidene fluoride (PVDF) membranes (HVLP06225, Millipore, Darmstadt, Germany). After blocking in 5% skimmed milk for 2 hours, membranes were incubated overnight at 4 °C with primary antibodies. The primary antibodies used were: rabbit anti-cGAS (1:1000, 31659), rabbit anti-STING (1:1000, 13647), rabbit anti-TBK1 (1:1000, 3504), rabbit anti-phospho-TBK1 (1:1000, 5483), rabbit anti-IRF3 (1:1000, 4302), rabbit anti-phospho-IRF3 (1:1000, 4947), rabbit anti-β-actin (1:1000, 4970), rabbit anti-GAPDH (1:1000, 5174, all from Cell Signaling Technology, Boston, MA, USA), rabbit anti-zonula occluden-1 (ZO-1) (1:1000, 61-7300, Invitrogen, Waltham, MA, USA), rabbit anti-occludin (1:1000, ab216327, Abcam, Cambridge, UK), rabbit anti-MBP (1:1000, ab40390, Abcam), goat anti-ionized calcium-binding adapter molecule 1 (Iba1) (1:1000, ab5076, Abcam), mouse anti-nonphosphorylated neurofilament-H (SMI-32, 1:1000, 801701, Biolegend, San Diego, CA, USA). Membranes were incubated with horseradish peroxidase-conjugated secondary antibodies for 2 hours at room temperature. Blots were visualized with Image Lab 6.0 software (Bio-Rad Laboratories, Hercules, CA, USA) and quantified using Image J software (1.8.0, NIH, Bethesda, MD, USA).

2.5 Immunofluorescence

Cold phosphate-buffered saline (PBS) was used to perfuse mice under deep anesthesia (isoflurane, 2%, R510-22-10, RWD Life Science), followed by 4% paraformaldehyde (PFA, 8187150100, Sigma-Aldrich). Brains were fixed with 4% PFA and then immersed in 20% and 30% sucrose at 4 °C overnight. Coronal sections of 20 µm thickness were blocked with the solution consisting

of 1% bovine serum albumin (BSA, V900933, Sigma-Aldrich), consisting 0.3% Triton X-100 (T9284, Sigma-Aldrich) and 3% donkey serum (D9663, Sigma-Aldrich) or goat serum (NS02L, Sigma-Aldrich) and then incubated overnight at 4 °C with primary antibodies: rabbit anti-cGAS (1:200), rabbit anti-STING (1:500, NBP2-24683, NOVUS Biologicals, Centennial, CO, USA), goat anti-Iba1 (1:800, ab5076, Abcam), rabbit anti-Iba1 (1:400, 019-19741, Wako, Osaka, Japan), goat anti-CD31 (1:200, AF3628, R&D Systems, Minneapolis, MN, USA), mouse anti-NeuN (1:1000, MAB377, Millipore), goat anti-GFAP (1:200, ab53554, Abcam), rat anti-CD16 (1:200, 553142, BD Biosciences, Franklin Lakes, NJ, USA), goat anti-CD206 (1:200, AF2535, R&D Systems), rabbit anti-MBP (1:800, ab40390, Abcam), mouse anti-nonphosphorylated neurofilament-H (SMI-32, 1:200, 801701, Biolegend). The second antibodies used were: Alexa Fluor 594-conjugated donkey anti-rabbit IgG (A-21207), Alexa Fluor 488conjugated donkey anti-goat IgG (A-11055), Alexa Fluor 594-conjugated donkey anti-rat IgG (A-21209), Alexa Fluor 594-conjugated donkey anti-goat IgG (A-11058), Alexa Fluor 488-conjugated donkey anti-mouse IgG (A-21202), Alexa Fluor 488-conjugated goat anti-rat IgG (A-11006), and Alexa Fluor 488-conjugated donkey anti-rabbit IgG (A-21206) (1:1000, all from Invitrogen, diluted in 1% BSA, consisting 0.3% Triton X-100 and 1% donkey or goat serum). Nuclei were stained with 4,6-Diamidino-2-phenylindole (DAPI, 1:10,000, 33342, Invitrogen). To measure the leakage of IgG, cerebral sections were incubated with blocking solution (1% BSA, 0.1% Triton X-100, and 5% donkey serum in PBS) for 2 h. Then, the sections were stained with goat anti-CD31 overnight at 4 °C. After washing in PBS, the sections were incubated with Alexa Fluor 594 donkey anti-goat IgG and Alexa Fluor 488conjugated donkey anti-mouse IgG for 1 h at room temperature. Brain sections were imaged using a fluorescence microscope (Axio Observer 7, ZEISS, Oberkochen, BW, Germany) equipped with a $\times 20$ or $\times 40$ objective lens. Specific filters were selected based on fluorophore conjugates, and uniform exposure times were set for each channel of all samples to ensure comparability. Then, images were captured with the same pixels and saved in TIFF format to preserve the integrity of the raw data. All images for a given antibody marker were acquired under identical microscope settings. For immunohistochemical quantification, three fields from the brain tissue (Fig. 1A) in three sections were captured under ×20 or ×40 objectives in each animal. Images were processed using ImageJ software and contrast-enhanced to differentiate positive signals from the background. The fluorescent density of MBP and SMI-32 was measured using the ImageJ plugin "integrated density" analysis tool. The number of cGAS⁺, STING⁺, Iba1⁺, CD16⁺Iba1⁺ and CD206⁺Iba1⁺ cells was examined using the ImageJ "Multi-point" measurement tool and was expressed as cells/mm². To quantify extravascular deposits



of IgG, the images were contrast-enhanced to differentiate positive signals from the background. The immunofluorescent density of extravascular IgG was measured using the ImageJ plugin "integrated density" analysis tool.

2.6 Y-Maze Test

The Y-maze test, as previously described, is employed to examine spatial working memory [23]. The device consists of three arms that diverge at 120 degrees from the central point. Mice were set in the center of the maze and given 5 minutes to move around freely. The experiment was completely videotaped with a camera, and the sequence of arm entries was analyzed by means of ANY-maze 7.4 software (Steolting, Wood Dale, IL USA). The percentage of spontaneous alternation was calculated using the following formula: (number of spontaneous alternation) / (total number of arm entries-2) × 100 [24].

2.7 Novel Object Recognition (NOR) Test

NOR test was used to assess cognitive memory in mice [25]. This test is divided into two different phases, including the training and testing parts, with a rest period between each phase. In the training phase, mice explored an openfield box with two identical objects for 10 minutes. During the testing stage, mice were placed in the same arena and exposed to two objects, one familiar and one novel object. All experiments were recorded via a video camera and analyzed using ANY-maze 7.4 software. The formula for the calculation of the recognition index is: novel object time/total object time ×100 [26].

2.8 Rotarod Test

The rotarod test was used to examine motor coordination of the mice as described previously [27]. Mice were placed on a rotarod cylinder (47650, Ugo Basile, Gemonio, Italy). The speed of rotarod was accelerated from 4 to 40 rpm within 5 minutes. The latency of falling was recorded, and three trials were conducted to calculate the average value. Before surgery, mice were trained for 3 consecutive days.

2.9 Statistical Analysis

Data are presented as means \pm standard deviations (SD) and were analyzed by using GraphPad Prism 9 software (Dotmatics, Boston, MA, USA). All data were tested for normality using the Shapiro-Wilk test. Because all data passed the normality test, differences between two groups were performed using unpaired Student' t test and multiple group comparisons were analyzed by one-way analysis of variance (ANOVA) followed by the Bonferroni multiple comparison test. A value of p < 0.05 was considered statistically significant.

3. Results

3.1 GMH Upregulated the Brain Expression of cGAS and STING

The protein levels of cGAS and STING in the hemorrhagic brain hemisphere were assessed at 24 h, 72 h, and 7 d after GMH. A significant increase in cGAS expression was observed at 24 and 72 h and peaked at 24 h post-GMH compared to the sham group (Fig. 1B,C). STING expression was significantly increased at 24 h post-GMH compared to sham (Fig. 1D,E). All original Western blot figures of Fig. 1B,D are available in Supplementary Material 1. Immunostaining revealed a marked increase in the number of cGAS⁺ and STING⁺ cells in the peri-hematomal area at 24 and 72 h after GMH compared to the sham-operated brains (Fig. 1F-H). Double immunostaining of cGAS and STING with Iba1 (microglial marker), NeuN (neuron marker), and GFAP (astrocyte marker) indicated that increased expression of cGAS and STING were colocalized with microglia, whereas only minimal cGAS and STING staining was observed in GFAP⁺ astrocytes and NeuN⁺ neurons (Fig. 1I,J).

3.2 Inhibition of cGAS Reduces Microglial Inflammation and Increases M2-Like Microglial Polarization After GMH

To investigate the effects of cGAS following GMH, mice were treated with RU.521, a small molecule that inhibits cGAS by attaching to its catalytic site and preventing its DNA-activated activity [16]. Western blots confirmed a decrease in cGAS expression in the peri-hematomal area in RU.521-treated mice compared to vehicle-treated mice (Supplementary Material 2 Fig. 1A,B). We then found that RU.521 reduced GMH-induced elevation of STING (Supplementary Material 2 Fig. 1C,D). Compared with sham group, microglial number was increased at 24 h after GMH (Fig. 2A,B). Treatment with RU.521 1 h following GMH resulted in a significant reduction in microglial number. Microglia activation leads to the synthesis and secretion of various inflammatory mediators, which contribute to the development of secondary brain damage [28]. We showed that mice treated with RU.521 exhibited significantly lower levels of IL-1 β , IL-6, and TNF α compared with vehicle-treated mice (Fig. 2C–E).

Neuroinflammation following stroke is primarily attributed to microglial polarization [29,30]. We found a marked upregulation in the levels of M1 phenotype factors (iNOS, CD86) and a moderate increase in the M2 phenotype factors (Arg-1 and CD206) at 24 h after GMH (Fig. 2F–I). We then observed that RU.521 decreased M1 phenotyperelated gene expression while enhancing M2 phenotyperelated gene expression. To further test the effects of cGAS inhibition on the M1/M2 polarization, we performed immunofluorescence staining for CD16 and CD206 together with Iba1. The study found that the number of CD16-positive microglia (M1-like microglia) increased after GMH and significantly decreased after RU.521 treat-



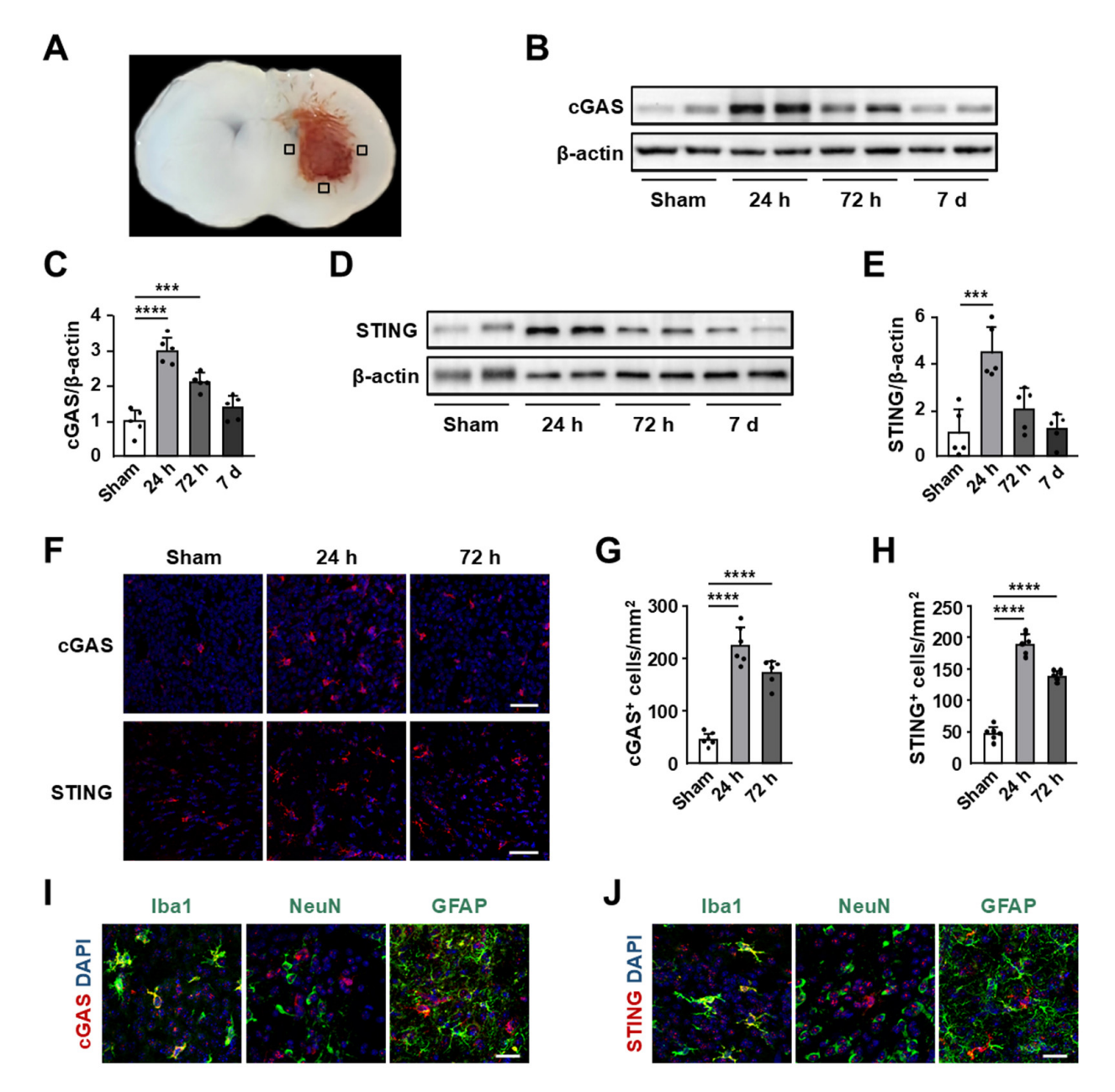


Fig. 1. Increased expression of cGAS and STING after GMH. (A) Representative photograph of coronal brain sections showing the location (black boxes) imaged for the cellular protein experiments in immunohistology. Imaging obtained from the similar parts of the brain in sham-operated mice and mice treated with vehicle, RU.521 or RU.521 in combination with SR-717 were used for comparison. (B–E) Representative immunoblots and quantification of cGAS (B,C) and STING (D,E) at 24 h, 72 h, and 7 d after GMH (n = 5). (F–H) Representative images (F) and quantification of cGAS (G) and STING (H) in the peri-hematomal area at 24 h (n = 6). Cell nuclei were stained with DAPI. Scale bar, 50 μm. (I,J) Double immunostaining of cGAS (I) and STING (J) with microglia (Iba1), neuron (NeuN) and astrocytes (GFAP). Cell nuclei were stained with DAPI. Scale bar, 20 μm. Values are mean \pm SD. ***p < 0.001, ****p < 0.0001. cGAS, cyclic GMP-AMP synthase; STING, stimulator of interferon genes; GMH, germinal matrix hemorrhage; DAPI, 4,6-Diamidino-2-phenylindole.

ment (Fig. 2J–M). Simultaneously, RU.521 significantly increased the number of CD206-positive microglia (M2-like microglia) after GMH compared with the vehicle group. These results suggest that RU.521 blunted the M1-like polarization and promoted the M2-like polarization of microglia after GMH.

3.3 Inhibition of cGAS Preserves BBB Integrity After GMH

BBB permeability was assessed at 24 h after GMH using IgG and the endothelial cell marker CD31. The findings indicated a notable rise in the perivascular IgG fluorescence density following GMH compared to the shamoperated group (Fig. 3A,B), suggesting disruption of the



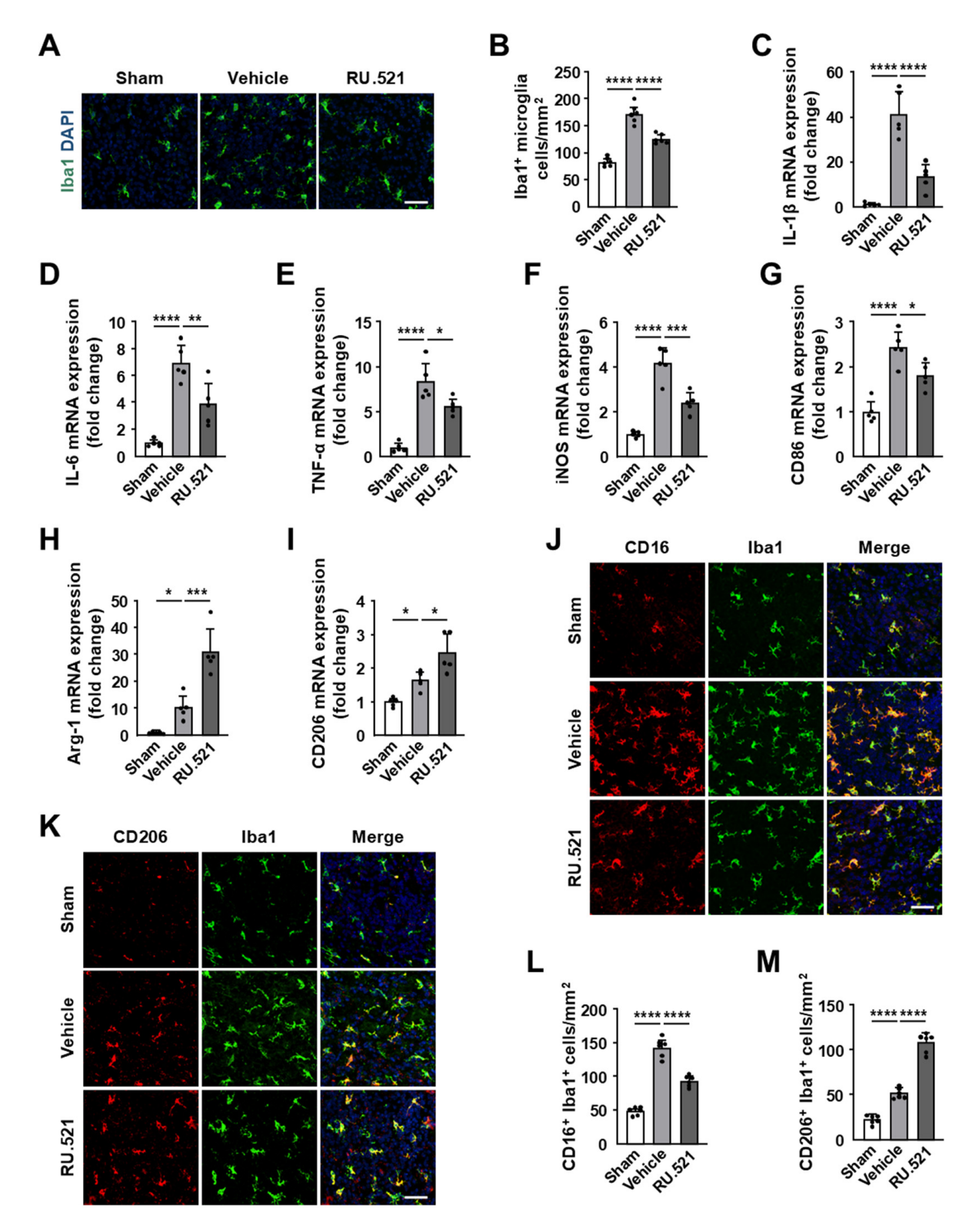


Fig. 2. Inhibition of cGAS by RU.521 reduces inflammation and drives M2 microglial polarization after GMH. (A,B) Representative images (A) and quantification (B) of Iba1⁺ microglia in the peri-hematomal area at 24 hours after GMH (n = 6). Cell nuclei were stained with DAPI. Scale bar, 50 μm. (C–E) Relative gene expression of *IL-1β* (C), *IL-6* (D), and *TNF-α* (E) (n = 5). (F–I) Relative gene expression of *iNOS* (F), *CD86* (G), *Arg-1* (H), and *CD206* (I) (n = 5). (J,K) Double immunostaining of CD16 (J) and CD206 (K) with microglia (Iba1). (L,M) Quantification of CD16⁺Iba⁺ pro-inflammatory microglia (L) and CD206⁺Iba1⁺ anti-inflammatory microglia (M) (n = 6). Nuclei were stained with DAPI. Scale bar, 50 μm. Values are mean \pm SD. *p < 0.05, **p < 0.01, ****p < 0.001. ****p < 0.0001. Arg-1, Arginase-1; IL-1β, Interleukin-1β; IL-6, Interleukin-6; TNF-α, Tumor necrosis factor-α; iNOS, inducible nitric oxide synthase; CD86, Cluster of differentiation 86.

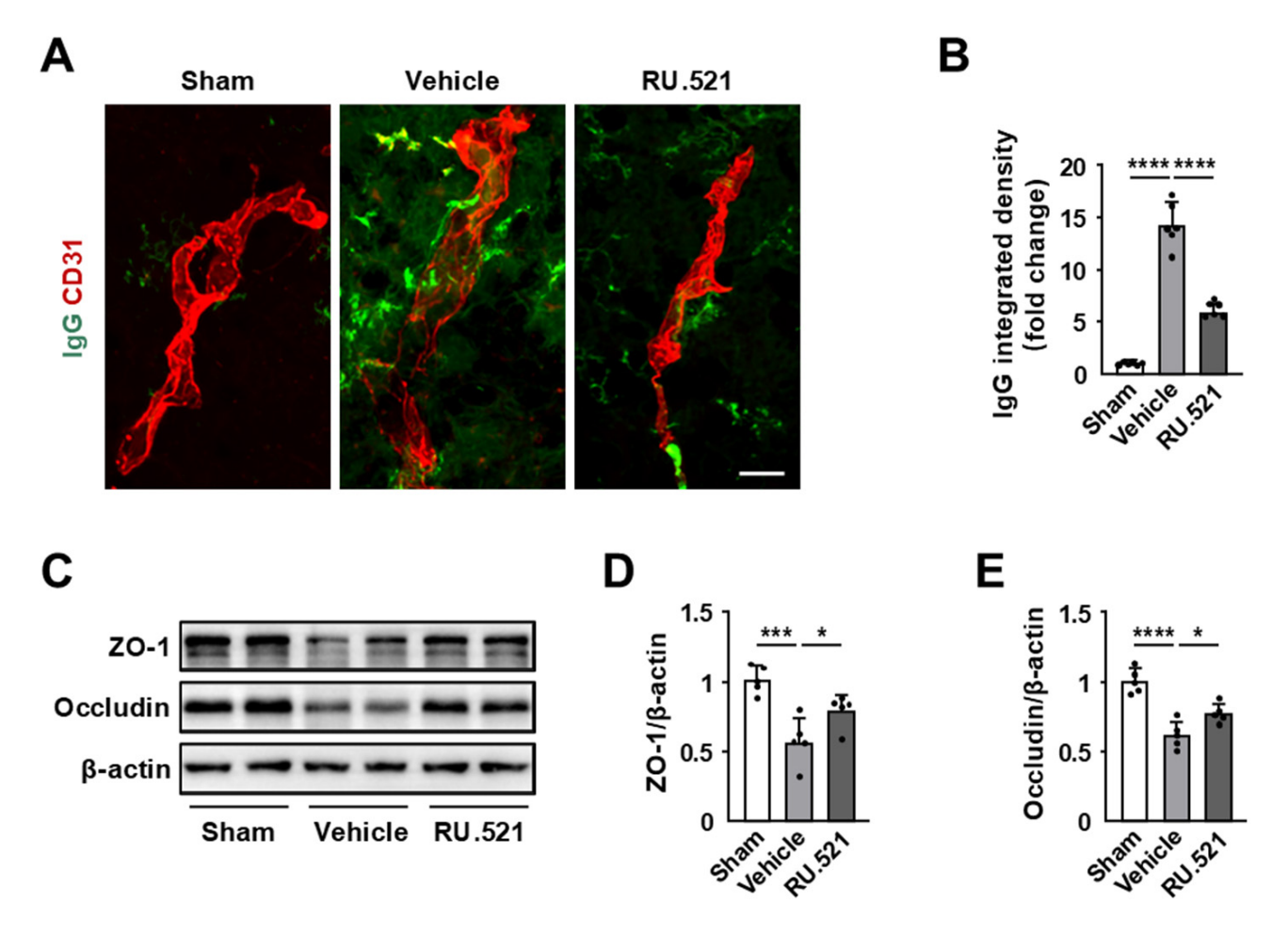


Fig. 3. The cGAS inhibitor RU.521 reduces blood-brain barrier disruption after GMH. (A,B) Representative images (A) and quantification (B) of IgG perivascular leakage at 24 hours after GMH in sham-operated mice and GMH mice treated with vehicle or RU.521 (n = 6). Microvessels were stained with CD31. Scale bar, 20 μ m. (C–E) Representative immunoblots (C) and quantification of tight junction proteins ZO-1 (D) and occludin (E) in the peri-hematomal area (n = 5). Values are mean \pm SD. *p < 0.05, ****p < 0.001, ****p < 0.0001. ZO-1, zonula occluden-1.

BBB. RU.521 administration significantly decreased extravascular IgG levels compared to vehicle-treated mice. We next investigated the impact of RU.521 on the degradation of BBB tight junction proteins. We found that RU.521 markedly reduced GMH-induced reduction of the tight junction proteins ZO-1 and occludin in the peri-hematomal regions (Fig. 3C–E). All original Western blot figures of Fig. 3C are available in **Supplementary Material 1.**

3.4 Inhibition of cGAS Reduces White Matter Injury and Improves Neurological Functions After GMH

At day 28 after GMH, western blot analysis revealed reduced expression of the myelin-associated protein (MBP) and elevated levels of the axonal marker SMI-32 in the corpus callosum compared to sham-operated mice (Fig. 4A–C, **Supplementary Material 2 Fig. 2A**). All original Western blot figures of Fig. 4A,C are available in **Supplementary Material 1**. Immunofluorescence quantification revealed that GMH mice exhibited significantly decreased MBP fluorescence intensity and increased SMI-32 staining intensity

in the corpus callosum compared to sham-operated mice (Fig. 4D-F, Supplementary Material 2 Fig. 2B). Novel object recognition test, Y-maze test, and rotarod test were used to assess long-term neurological deficits in mice subjected to sham operation and GMH at 28 days after GMH. In the novel object recognition test, GMH mice exhibited a significant decrease in the exploration time for novel objects, as indicated by the recognition index (Fig. 4G). In the Y-maze test, GMH mice exhibited fewer spontaneous alternations, indicating an impairment in working memory (Fig. 4H). The rotarod test showed that locomotor activity was impaired in mice subjected to GMH (Fig. 4I). Treatment with RU.521 enhanced MBP and SMI-32 expression and fluorescence intensity, suggesting decreased demyelination and axonal degeneration. Consistent with these findings, cognitive function and working memory were improved in mice treated with RU.521.



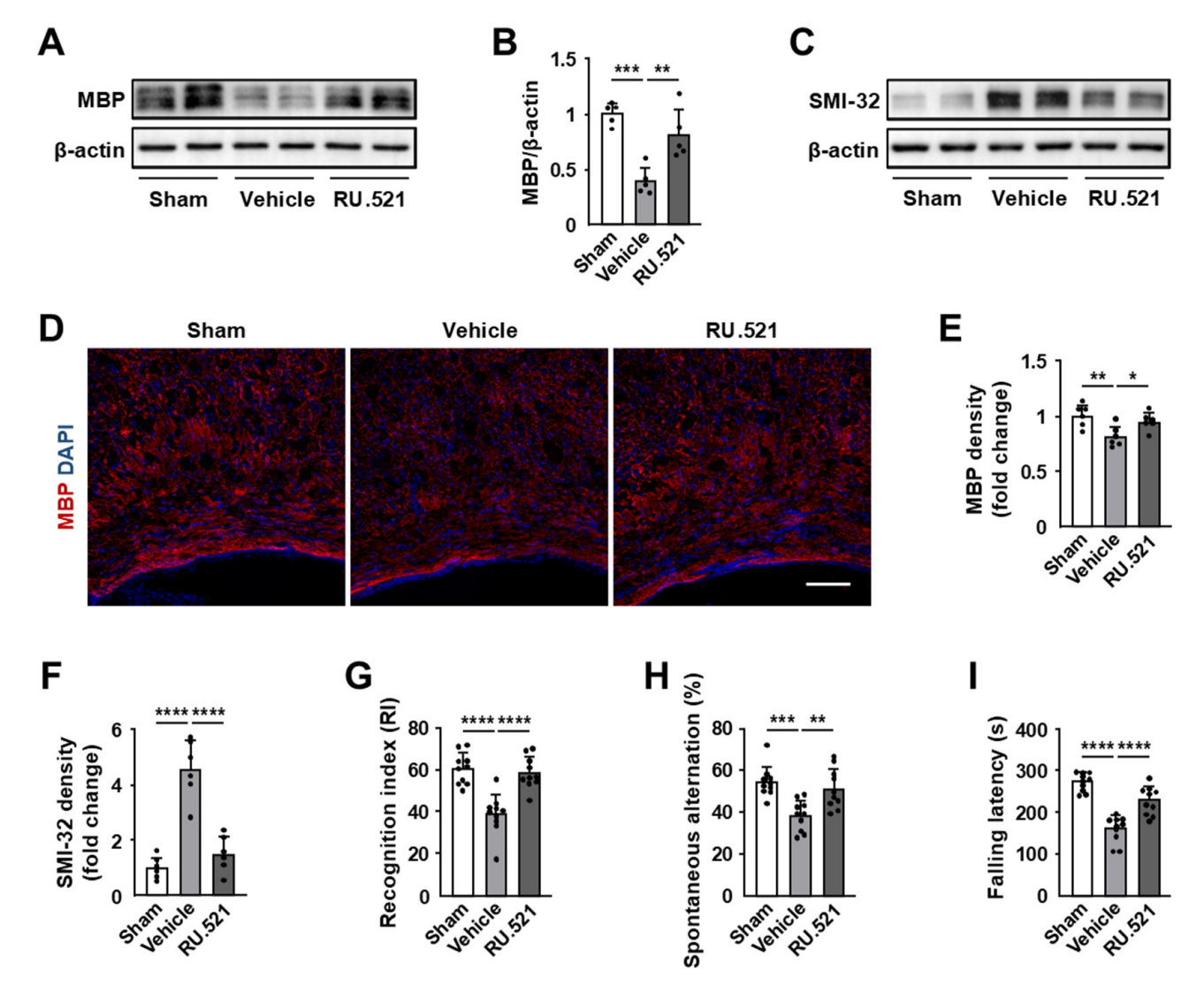


Fig. 4. RU.521 improves white matter injury and behavioral function after GMH. (A,B) Representative immunoblots (A) and quantification (B) of MBP in the corpus callosum at day 28 after GMH (n = 5). (C) Representative immunoblots of SMI-32 in the corpus callosum (n = 5). (D,E) Representative images (D) and quantification of MBP (E) fluorescence density in the corpus callosum (n = 6). Nuclei were stained with DAPI. Scale bar, 100 μ m. (F) Quantification of SMI-32 fluorescence density in the corpus callosum (n = 6). (G–I) RU.521 improved behavioral outcomes in the novel object recognition test (G), Y-maze test (H), and rotarod test (I) (n = 10). Values are mean \pm SD. *p < 0.05, **p < 0.01, ****p < 0.001, ****p < 0.0001.

3.5 Inhibition of cGAS Reduces Inflammation, BBB Disruption and White Matter Injury via STING/p-TBK1/p-IRF3/IFN-β Signaling Pathway

The expression of downstream signaling molecules of cGAS was evaluated in the peri-hematomal area by Western blots at 24 h after GMH [31]. We observed robust induction of phospho-TBK1 and phospho-IRF3 (Fig. 5A–C) in GMH mice. All original Western blot figures of Fig. 5A are available in **Supplementary Material 1**. We then detected a marked increase in the levels of IFN- β (Fig. 5D), indicating STING pathway activation [32]. Treatment with the cGAS inhibitor RU.521 reduced GMH-induced activation of TBK1 and IRF3, as well as levels of IFN- β .

Our subsequent test was to determine whether RU.521's beneficial impact on GMH-induced damage operates via STING pathways specifically. Western blot analysis indicated that the STING agonist SR-717 reversed RU.521-mediated downregulation of STING (Fig. 5E,F), inactivation of TBK1 and IRF3 (Fig. 5G, Supplementary Material 2 Fig. 3A,B), and efficiently increased the levels of IFN-β after RU.521 treatment (Fig. 5H). All original Western blot figures of Fig. 5A,G are available in Supplementary Material 1. Furthermore, treatment with SR-717 dramatically increased the amount of microglia (Fig. 6A,B) and the levels of proinflammatory cytokines in the peri-hematomal area in mice treated with RU.521 (Fig. 6C–E). Previous study demonstrated that adminis-



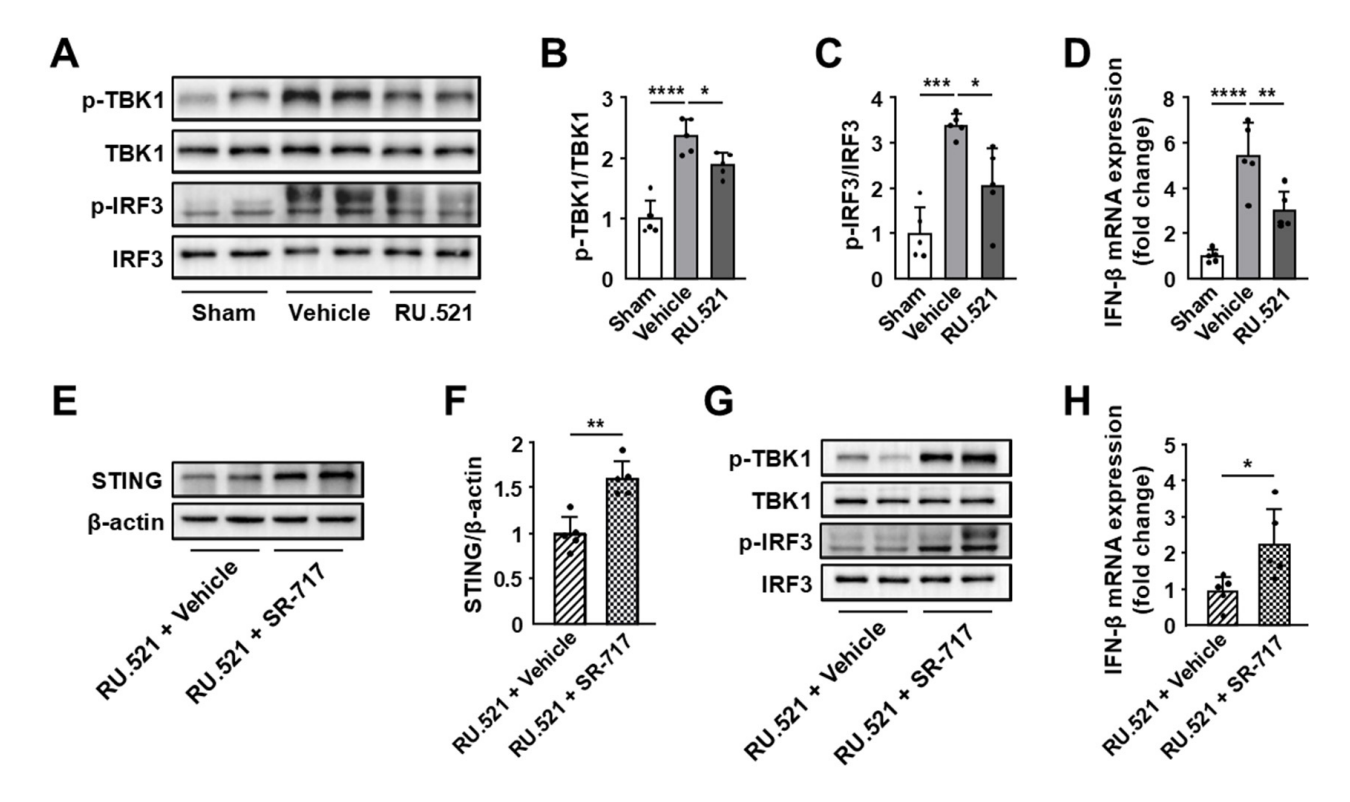


Fig. 5. Effects of RU.521 and the STING agonist-SR-717 on the expression of pTBK1, pIRF3 and IFN- β after GMH. (A) Representative immunoblots of phosphorylated TBK1 (pTBK1) and total TBK1, phosphorylated IRF3 (pIRF3) and total IRF3 in the perihematomal area at 24 hours after GMH in sham-operated mice and GMH mice treated with vehicle or RU.521. (B,C) Quantification of pTBK1 (B) and pIRF3 (C) band intensities (n = 5). (D) Relative gene expression of *IFN*- β (n = 5). (E,F) Representative immunoblots (E) and quantification (F) of STING in GMH mice treated with RU.521 or RU.521 in combination with SR-717 (n = 5). (G) Representative immunoblots of pTBK1, total TBK1, pIRF3 and total IRF3. (H) Relative gene expression of *IFN*- β (n = 5). Values are mean \pm SD. *p < 0.05, **p < 0.01, ***p < 0.001, ****p < 0.0001.

tration of SR-717 increased plasma levels of IFN- β and IL-6 in naïve mice [33]. To test whether SR-717 alone could influence neuroinflammation, we injected SR-717 intraperitoneally into sham-operated mice. Our results indicated that there was no difference in the expression of Iba1 protein between vehicle-treated and SR-717-treated sham-operated mice (Fig. 6A,B). All original Western blot figures of Fig. 6A are available in **Supplementary Material 1**. In addition, SR-717 did not significantly change the levels of IL-1 β , IL-6, and TNF- α in sham-operated mice (Fig. 6C–E). These findings are consistent with a report showing that hippocampal injection of cGAMP did not affect neuroinflammation compared with mice treated with vehicle [34].

We observed a significant downregulation of the tight junction proteins ZO-1 and occludin in mice treated with RU.521 and SR-717 compared to mice treated with RU.521 alone (Fig. 6F,G, Supplementary Material 2 Fig. 4A). All original Western blot figures of Fig. 6F are available in Supplementary Material 1. Immunofluorescence quantification showed a significant increase in the perivascular IgG fluorescence density treated with both RU.521 and SR-717, compared to those treated solely with RU.521 (Fig. 6H, Supplementary Material 2 Fig. 4B). Western blotting

showed that SR-717 reversed RU.521-mediated increase in the expression of MBP and decrease in the expression of SMI-32 in the corpus callosum at day 28 after GMH (Fig. 7A–C). All original Western blot figures of Fig. 7A are available in **Supplementary Material 1**. Immunofluorescence quantification of MBP and SMI-32 showed that SR-717 blocked RU.521-provided protection against demyelination (Fig. 7D,E) and axon degeneration (Fig. 7D,F). Consistent with these observations, we found that SR-717 exacerbated neurological outcomes in RU.521-treated mice, as shown by novel object recognition test, Y-maze test, and rotarod test (Fig. 7G–I).

4. Discussion

In the present study, we reported the importance of cGAS signaling pathway in GMH. We showed that inhibition of cGAS by RU.521 resulted in reduced neuroinflammation and BBB disruption. These effects were accompanied by decreased white matter lesions and improved neurobehavioral performance. Furthermore, we demonstrated that RU.521-afforded protective role on brain injury and neurological dysfunction after GMH was reversed by the STING agonist SR-717.



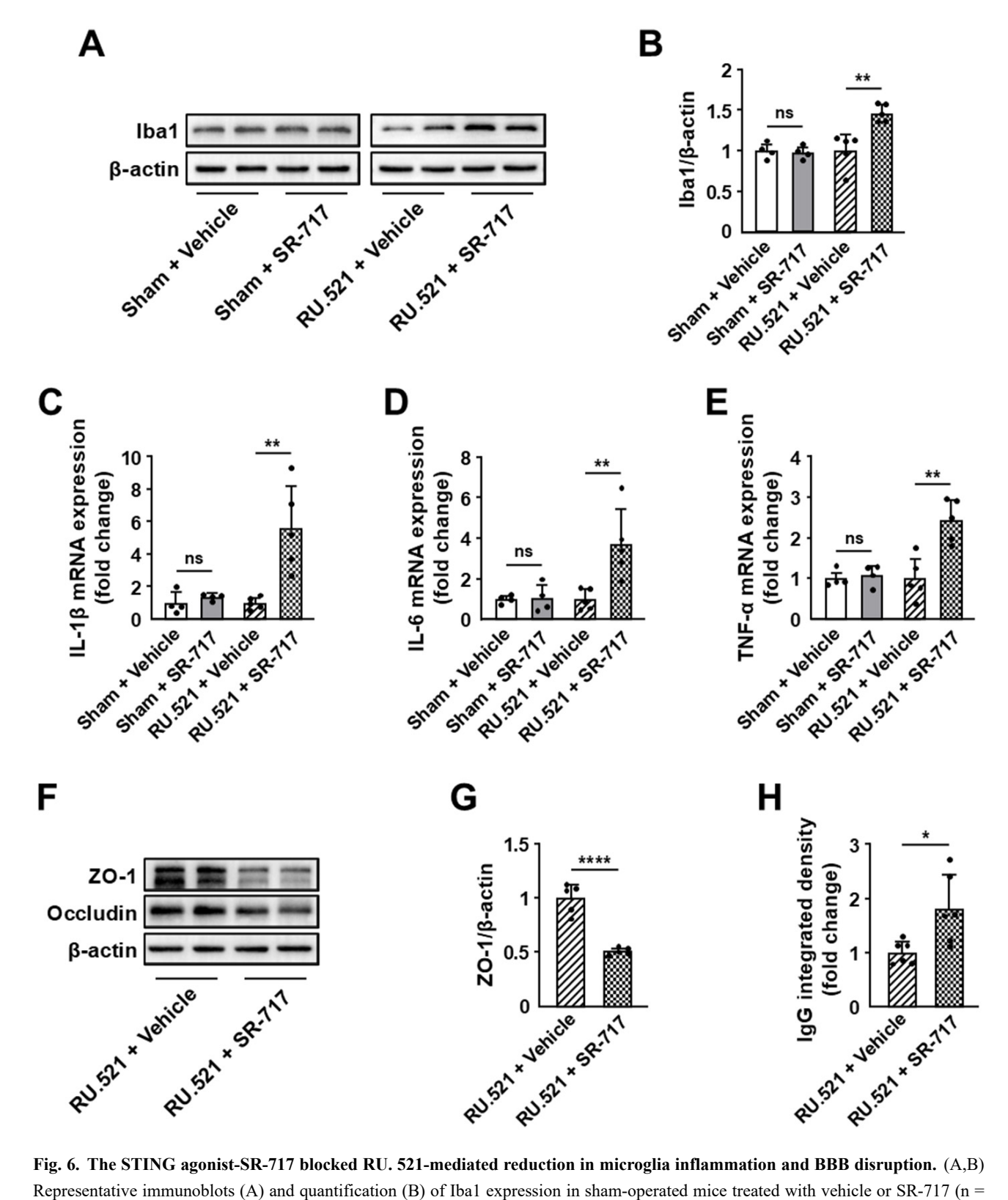


Fig. 6. The STING agonist-SR-717 blocked RU. 521-mediated reduction in microglia inflammation and BBB disruption. (A,B) Representative immunoblots (A) and quantification (B) of Iba1 expression in sham-operated mice treated with vehicle or SR-717 (n = 4) and in GMH mice treated with RU.521 or RU.521 in combination with SR-717 (n = 5). (C–E) Relative gene expression of IL-IB (C), IL-IB (D), and IB-IB (E) (n = 4–5). (F) Representative immunoblots ZO-1 and occludin (n = 5). (G) Quantification of ZO-1 (n = 5). (H) Quantification of IgG leakage (n = 6). Values are mean \pm SD. ns, not significant, \pm 0 0.05, \pm 0 0.01, \pm 0 0.001.

Inflammation is one of the typical features of GMH and serves as a trigger for secondary brain injury after GMH

[35]. Microglia, the resident immune cells in the CNS, are known to play a central role in the release of inflammatory

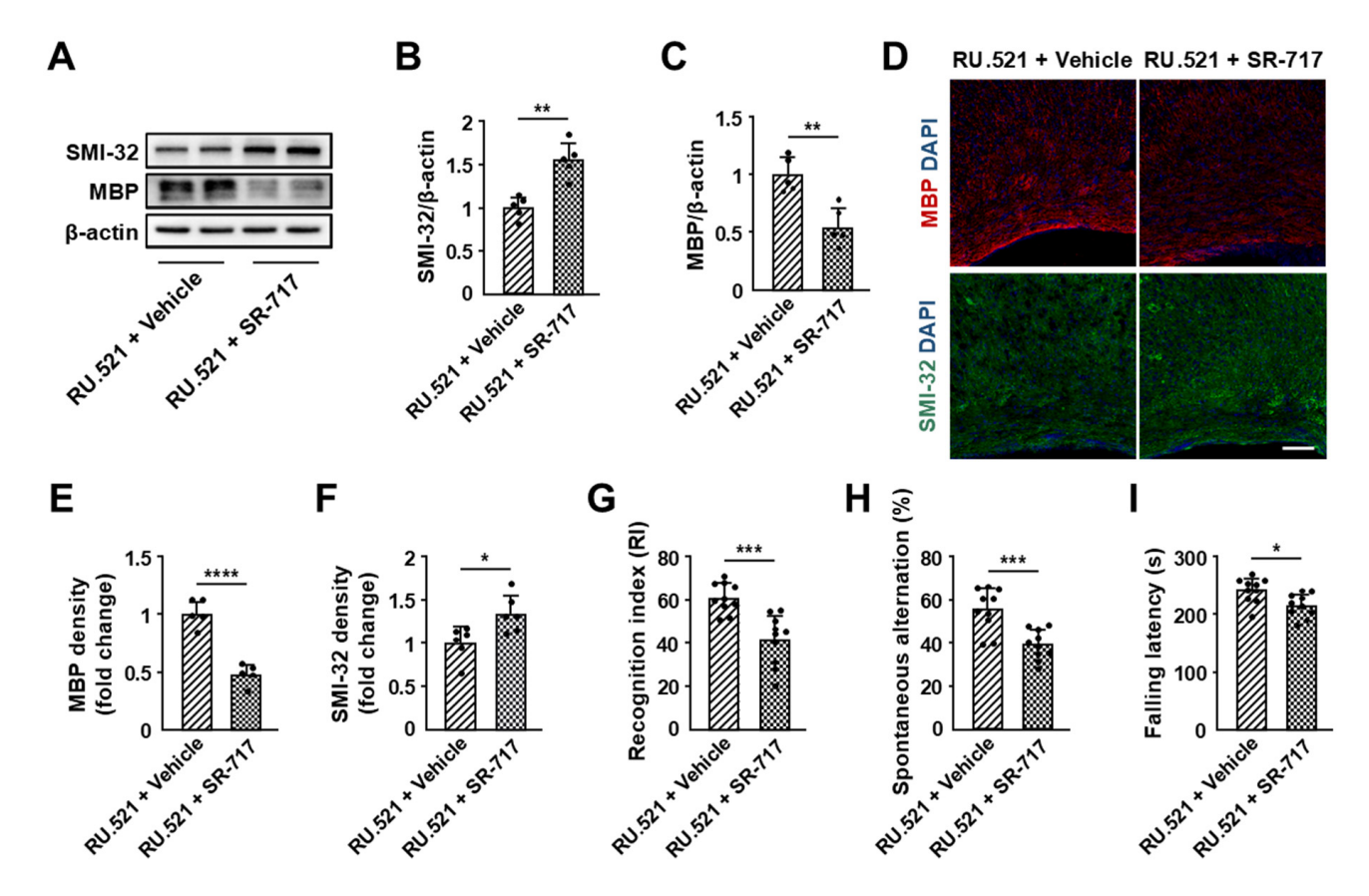


Fig. 7. RU.521-afforded protection on white matter lesions and behavioral outcomes were abolished by the STING agonist-SR-717. (A–C) Representative immunoblots (A) and quantification of SMI-32 (B) and MBP (C) expression in the corpus callosum at day 28 after GMH (n = 5). (D–F) Representative immunostaining (D) and quantification of MBP (E) and SMI-32 (F) fluorescence density in the corpus callosum (n = 6). Nuclei were stained with DAPI. Scale bar, 100 μ m. (G–I) Novel object recognition test (G), Y-maze test (H), and rotarod test (I) in mice treated with RU.521 or RU.521 in combination with SR-717 (n = 10). Values are mean \pm SD. *p < 0.05, **p < 0.01, ***p < 0.001, ****p < 0.0001.

cytokines after GMH [36]. The present study demonstrated that cGAS and the adapter STING were upregulated after GMH and were expressed mostly in microglia, suggesting that cGAS-STING pathway may play a role in GMHmediated microglial inflammation. Indeed, we observed that inhibition of cGAS using a potent small-molecule inhibitor RU.521 resulted in a significant reduction in the number of microglia and the levels of inflammatory cytokines (IL-1 β , IL-6, TNF- α). Furthermore, we evaluated the effect of RU.521 on microglial M1 and M2 polarization. Consistent with a previous study [37], our results showed predominantly promoted M1-like microglia polarization and moderately increased M2-like microglia polarization after GMH. Treatment with RU.521 significantly reduced pro-inflammatory cytokines and CD16-positive microglia with increased anti-inflammatory cytokines and CD206positive microglia after GMH, suggesting blunted M1-like microglia polarization and promoted M2-like microglia polarization.

The BBB integrity is critical for proper function of the neonatal brain [38], and inflammation contributes to cere-

brovascular dysfunction and BBB disruption [39]. Previous studies have shown that inflammation and high BBB permeability were associated with white matter injury and consequent functional outcomes [40,41]. Our findings showed that RU.521 treatment reduced degradation of the BBB tight junction proteins and thereby offered protection against BBB breakdown. These effects of RU.521 were followed by reduced demyelination and axon degeneration in the corpus callosum and less severe neurologic deficits.

As a cytoplasmic nucleic acid sensor, cGAS promotes STING-dependent type I IFN synthesis to trigger a variety of inflammatory responses [42]. We found that GMH significantly upregulated the levels of the STING downstream signals, including phospho-TBK1, phospho-IRF3, and IFN- β , in the injured brain. We then demonstrated that RU.521 inhibited STING pathway activation and IFN- β production, which were abolished by the STING agonist SR-717. Furthermore, SR-717 treatment blocked RU.521-mediated reduction in microglia and pro-inflammatory cytokines in the peri-hematomal area after GMH. We also observed that SR-717 increased BBB permeability in RU.521-



treated mice. Correspondingly, treatment with SR-717 reversed the protective effects of RU.521 against white matter lesions and worsened neurological outcomes in RU.521-treated mice. These results suggest that the beneficial roles of RU.521 on GMH were largely mediated by its ability to inhibit STING and its downstream signaling cascade.

There are some limitations in this current study. First, cGAS is primarily activated through an intrinsic mechanism involving cytosolic DNA fragments, which serve as a secondary trigger for the inflammatory response in most brain injuries. Previous research has shown that blood component enhanced production of the cytokines TNF- α and IL-6 by microglia [43]. A recent study demonstrated that hemoglobin promoted the inflammatory response following intraventricular hemorrhage [44]. Additionally, cell surface antigen, including T cell receptor-MHC and CD22 signaling, have also been implicated in the inflammatory response after brain injuries [45,46]. However, our study only focused on the effects of cGAS on microglia-mediated inflammatory response after GMH. Thus, we cannot exclude that the inhibition of other inflammatory pathways by RU.521 may also contribute to the improved cognitive function. Second, because of the limited sample size in per experimental group, statistical analyses were not performed to assess whether there were sex differences in RU.521afforded protection against GMH-induced brain damage. Future studies should increase the sample size to evaluate sex-based differences. Last, upregulation of cGAS has been closely linked with microglial activation after brain injury [47]. The use of RU.521 to inhibit the cGAS pathway activation was reported to effectively reduce microglia activation after subarachnoid hemorrhage, cerebral venous sinus thrombosis, and spared nerve injury [31,48,49]. We found that RU.521 treatment lessened the number of microglia and reduced neuroinflammation. However, because RU.521 is a more potent inhibitor against murine GAS than human GAS, caution should be taken in extrapolating the results to GMH patients in general.

5. Conclusions

In summary, the current study found that inhibition of cGAS improved white matter lesions by modulating the microglial polarization towards decreased inflammation and maintaining BBB integrity through STING-mediated type I IFN- β production. Our data suggest that cGAS may be a potential therapeutic target to improve GMH-associated brain injury and the resulting functional outcomes.

Availability of Data and Materials

The datasets used and analyzed during the current study are available from the corresponding author on reasonable request.

Author Contributions

YW: Writing – original draft, Writing – review & editing, Visualization, Methodology, Formal analysis, Data curation, Conceptualization. XY: Writing – review & editing, Data curation, Software. XLZ: Writing – review & editing, Data curation, Software. XXZ: Writing – review & editing, Data curation. YL: Writing – review & editing, Formal analysis. BZ: Writing – review & editing, Supervision, Resources, Methodology, Conceptualization, Funding acquisition. All authors read and approved the final manuscript. All authors have participated sufficiently in the work and agreed to be accountable for all aspects of the work.

Ethics Approval and Consent to Participate

All animal experiments were approved by the Animal Ethics Committee of the Third Affiliated Hospital of Zhengzhou University (Ethic Approval number: 2024-352-01). All the animal procedures were performed in accordance with the ARRIVE guidelines. Every procedure involving animals was completed in accordance with the institutional rules for animal welfare and authorized protocols.

Acknowledgment

Not applicable.

Funding

This research was funded by the Third Affiliated Hospital, Zhengzhou University (2023013).

Conflict of Interest

The authors declare no conflict of interest.

Supplementary Material

Supplementary material associated with this article can be found, in the online version, at https://doi.org/10.31083/JIN39286.

References

- [1] Santhosh D, Sherman J, Chowdhury S, Huang Z. Harnessing region-specific neurovascular signaling to promote germinal matrix vessel maturation and hemorrhage prevention. Disease Models & Mechanisms. 2019; 12: dmm041228. https://doi.org/10.1242/dmm.041228.
- [2] Atienza-Navarro I, Alves-Martinez P, Lubian-Lopez S, Garcia-Alloza M. Germinal Matrix-Intraventricular Hemorrhage of the Preterm Newborn and Preclinical Models: Inflammatory Considerations. International Journal of Molecular Sciences. 2020; 21: 8343. https://doi.org/10.3390/ijms21218343.
- [3] Alshareef M, Hatchell D, Vasas T, Mallah K, Shingala A, Cutrone J, *et al.* Complement Drives Chronic Inflammation and Progressive Hydrocephalus in Murine Neonatal Germinal Matrix Hemorrhage. International Journal of Molecular Sciences. 2023; 24: 10171. https://doi.org/10.3390/ijms241210171.
- [4] Alshareef M, Mallah K, Vasas T, Alawieh A, Borucki D, Couch C, et al. A Role of Complement in the Pathogenic Sequelae



- of Mouse Neonatal Germinal Matrix Hemorrhage. International Journal of Molecular Sciences. 2022; 23: 2943. https://doi.org/10.3390/ijms23062943.
- [5] Ballabh P, de Vries LS. White matter injury in infants with intraventricular haemorrhage: mechanisms and therapies. Nature Reviews. Neurology. 2021; 17: 199–214. https://doi.org/10.1038/s41582-020-00447-8.
- [6] Nilsson G, Baburamani AA, Rutherford MA, Zhu C, Mallard C, Hagberg H, et al. White matter injury but not germinal matrix hemorrhage induces elevated osteopontin expression in human preterm brains. Acta Neuropathologica Communications. 2021; 9: 166. https://doi.org/10.1186/s40478-021-01267-7.
- [7] Xue YX, Chen YJ, Qin MZ, Shang FF, Lu YT, Sun YH, *et al.* Microglial STING activation promotes neuroinflammation and pathological changes in experimental mice with intracerebral haemorrhage. Acta Pharmacologica Sinica. 2025. https://doi.org/10.1038/s41401-025-01540-8. (online ahead of print)
- [8] Gamdzyk M, Doycheva DM, Araujo C, Ocak U, Luo Y, Tang J, et al. cGAS/STING Pathway Activation Contributes to Delayed Neurodegeneration in Neonatal Hypoxia-Ischemia Rat Model: Possible Involvement of LINE-1. Molecular Neurobiology. 2020; 57: 2600–2619. https://doi.org/10.1007/ s12035-020-01904-7.
- [9] Paul BD, Snyder SH, Bohr VA. Signaling by cGAS-STING in Neurodegeneration, Neuroinflammation, and Aging. Trends in Neurosciences. 2021; 44: 83–96. https://doi.org/10.1016/j.tins .2020.10.008.
- [10] Wang R, Zhu Y, Liu Z, Chang L, Bai X, Kang L, et al. Neutrophil extracellular traps promote tPA-induced brain hemorrhage via cGAS in mice with stroke. Blood. 2021; 138: 91–103. https://doi.org/10.1182/blood.2020008913.
- [11] Jiang GL, Yang XL, Zhou HJ, Long J, Liu B, Zhang LM, et al. cGAS knockdown promotes microglial M2 polarization to alleviate neuroinflammation by inhibiting cGAS-STING signaling pathway in cerebral ischemic stroke. Brain Research Bulletin. 2021; 171: 183–195. https://doi.org/10.1016/j.brainresbu II.2021.03.010.
- [12] Li B, Wang W, Li Y, Wang S, Liu H, Xia Z, et al. cGAS-STING pathway aggravates early cerebral ischemia-reperfusion injury in mice by activating NCOA4-mediated ferritinophagy. Experimental Neurology. 2023; 359: 114269. https://doi.org/10.1016/ j.expneurol.2022.114269.
- [13] Liao Y, Cheng J, Kong X, Li S, Li X, Zhang M, et al. HDAC3 inhibition ameliorates ischemia/reperfusion-induced brain injury by regulating the microglial cGAS-STING pathway. Theranostics. 2020; 10: 9644–9662. https://doi.org/10.7150/thno.47651.
- [14] Hu X, Zhang H, Zhang Q, Yao X, Ni W, Zhou K. Emerging role of STING signalling in CNS injury: inflammation, autophagy, necroptosis, ferroptosis and pyroptosis. Journal of Neuroinflammation. 2022; 19: 242. https://doi.org/10.1186/s12974-022-02602-y.
- [15] Xie W, Lama L, Adura C, Tomita D, Glickman JF, Tuschl T, et al. Human cGAS catalytic domain has an additional DNA-binding interface that enhances enzymatic activity and liquid-phase condensation. Proceedings of the National Academy of Sciences of the United States of America. 2019; 116: 11946–11955. https://doi.org/10.1073/pnas.1905013116.
- [16] Vincent J, Adura C, Gao P, Luz A, Lama L, Asano Y, et al. Small molecule inhibition of cGAS reduces interferon expression in primary macrophages from autoimmune mice. Nature Communications. 2017; 8: 750. https://doi.org/10.1038/s41467-017-00833-9.
- [17] Hatchell D, Alshareef M, Vasas T, Guglietta S, Borucki D, Guo C, et al. A role for P-selectin and complement in the pathological sequelae of germinal matrix hemorrhage. Journal of Neuroinflammation. 2023; 20: 143. https://doi.org/10.1186/

- s12974-023-02828-4.
- [18] Xu Q, Xiong H, Zhu W, Liu Y, Du Y. Small molecule inhibition of cyclic GMP-AMP synthase ameliorates sepsis-induced cardiac dysfunction in mice. Life Sciences. 2020; 260: 118315. https://doi.org/10.1016/j.lfs.2020.118315.
- [19] Lin C, He C, Li L, Liu Y, Tang L, Ni Z, et al. Alpha-lipoic acid (ALA) ameliorates early brain injury after subarachnoid hemorrhage in Sprague-Dawley (SD) rats via inhibiting STING-NLRP3 inflammatory signaling. Neuroreport. 2024; 35: 250– 257. https://doi.org/10.1097/WNR.0000000000001998.
- [20] Jiang Y, Wang N, Liu J, Li J, Chang L, Yang C, et al. Evobrutinib mitigates neuroinflammation after ischemic stroke by targeting M1 microglial polarization via the TLR4/Myd88/NF-κB pathway. Molecular Medicine. 2025; 31: 148. https://doi.org/10.1186/s10020-025-01203-8.
- [21] Wang B, Chen J, Wang S, Chen L, Zhang X, Zhou T, et al. Kv1.3 Blockade Alleviates White Matter Injury through Reshaping M1/M2 Phenotypes via the NF-κB Signaling Pathway after Intracerebral Hemorrhage. Journal of Integrative Neuroscience. 2023; 22: 171. https://doi.org/10.31083/j.jin2206171.
- [22] Deng H, Zhang Y, Li GG, Yu HH, Bai S, Guo GY, et al. P2X7 receptor activation aggravates NADPH oxidase 2-induced oxidative stress after intracerebral hemorrhage. Neural Regeneration Research. 2021; 16: 1582–1591. https://doi.org/10.4103/1673-5374.303036.
- [23] Yang X, Chang L, Liu Z, Geng X, Wang R, Yin X, et al. Neddylation in the chronically hypoperfused corpus callosum: MLN4924 reduces blood-brain barrier injury via ERK5/KLF2 signaling. Experimental Neurology. 2024; 371: 114587. https://doi.org/10.1016/j.expneurol.2023.114587.
- [24] Yang EJ, Cai M, Lee JH. Neuroprotective Effects of Electroacupuncture on an Animal Model of Bilateral Common Carotid Artery Occlusion. Molecular Neurobiology. 2016; 53: 7228–7236. https://doi.org/10.1007/s12035-015-9610-7.
- [25] Shi X, Bai H, Wang J, Wang J, Huang L, He M, et al. Behavioral Assessment of Sensory, Motor, Emotion, and Cognition in Rodent Models of Intracerebral Hemorrhage. Frontiers in Neurology. 2021; 12: 667511. https://doi.org/10.3389/fneur.2021.667511.
- [26] Cai M, Shin BY, Kim DH, Kim JM, Park SJ, Park CS, et al. Neuroprotective effects of a traditional herbal prescription on transient cerebral global ischemia in gerbils. Journal of Ethnopharmacology. 2011; 138: 723–730. https://doi.org/10.1016/j.jep. 2011.10.016.
- [27] Alves-Martinez P, Atienza-Navarro I, Vargas-Soria M, Carranza-Naval MJ, Infante-Garcia C, Benavente-Fernandez I, et al. Caffeine Restores Neuronal Damage and Inflammatory Response in a Model of Intraventricular Hemorrhage of the Preterm Newborn. Frontiers in Cell and Developmental Biology. 2022; 10: 908045. https://doi.org/10.3389/fcell.2022.908045.
- [28] Dienel A, Veettil RA, Matsumura K, Savarraj JPJ, Choi HA, Kumar T P, et al. α₇-Acetylcholine Receptor Signaling Reduces Neuroinflammation After Subarachnoid Hemorrhage in Mice. Neurotherapeutics. 2021; 18: 1891–1904. https://doi.org/ 10.1007/s13311-021-01052-3.
- [29] Xu N, Li X, Weng J, Wei C, He Z, Doycheva DM, et al. Adiponectin Ameliorates GMH-Induced Brain Injury by Regulating Microglia M1/M2 Polarization Via AdipoR1/APPL1/AMPK/PPARγ Signaling Pathway in Neonatal Rats. Frontiers in Immunology. 2022; 13: 873382. https://doi.org/10.3389/fimmu.2022.873382.
- [30] Liu W, Man X, Wang Y, Wang Q, Wang Z, Qi J, et al. Tirofiban mediates neuroprotective effects in acute ischemic stroke by reducing inflammatory response. Neuroscience. 2024; 555: 32– 40. https://doi.org/10.1016/j.neuroscience.2024.07.016.
- [31] Shao J, Meng Y, Yuan K, Wu Q, Zhu S, Li Y, et al. RU.521



- mitigates subarachnoid hemorrhage-induced brain injury via regulating microglial polarization and neuroinflammation mediated by the cGAS/STING/NF-kB pathway. Cell Communication and Signaling. 2023; 21: 264. https://doi.org/10.1186/s12964-023-01274-2.
- [32] Wu J, Sun L, Chen X, Du F, Shi H, Chen C, et al. Cyclic GMP-AMP is an endogenous second messenger in innate immune signaling by cytosolic DNA. Science. 2013; 339: 826– 830. https://doi.org/10.1126/science.1229963.
- [33] Chin EN, Yu C, Vartabedian VF, Jia Y, Kumar M, Gamo AM, et al. Antitumor activity of a systemic STING-activating non-nucleotide cGAMP mimetic. Science. 2020; 369: 993–999. https://doi.org/10.1126/science.abb4255.
- [34] Wang Y, Niu W, Zhu S, Sun J, Lv J, Wang N, et al. STING Agonist cGAMP Attenuates Sleep Deprivation-Induced Neuroin-flammation and Cognitive Deficits via TREM2 Up-Regulation. Inflammation. 2024; 47: 2129–2144. https://doi.org/10.1007/s10753-024-02029-y.
- [35] Agyemang AA, Sveinsdóttir K, Vallius S, Sveinsdóttir S, Bruschettini M, Romantsik O, et al. Cerebellar Exposure to Cell-Free Hemoglobin Following Preterm Intraventricular Hemorrhage: Causal in Cerebellar Damage? Translational Stroke Research. 2017; 8: 461–473. https://doi.org/10.1007/s12975-017-0539-1. (online ahead of print)
- [36] Yin X, Wang Y, Zhang X, Zhu X, Zhao BQ. Protective effects of alectinib on germinal matrix hemorrhage-induced neonatal brain injury. NeuroReport. 2025; 36: 599–608. https://doi.org/10.1097/WNR.0000000000002180.
- [37] Tao Y, Li L, Jiang B, Feng Z, Yang L, Tang J, *et al.* Cannabinoid receptor-2 stimulation suppresses neuroinflammation by regulating microglial M1/M2 polarization through the cAMP/PKA pathway in an experimental GMH rat model. Brain, Behavior, and Immunity. 2016; 58: 118–129. https://doi.org/10.1016/j.bbi.2016.05.020.
- [38] Li W, Zou J, Shang J, Gao C, Sun R, Liu R, et al. Both the Complexity of Tight Junctions and Endothelial Transcytosis Are Increased During BBB Postnatal Development in Rats. Frontiers in Neuroscience. 2022; 16: 850857. https://doi.org/10.3389/fnins.2022.850857.
- [39] Candelario-Jalil E, Dijkhuizen RM, Magnus T. Neuroinflammation, Stroke, Blood-Brain Barrier Dysfunction, and Imaging Modalities. Stroke. 2022; 53: 1473–1486. https://doi.org/10.1161/STROKEAHA.122.036946.
- [40] Meng S, Cao H, Huang Y, Shi Z, Li J, Wang Y, et al. ASK1-K716R reduces neuroinflammation and white matter injury via

- preserving blood-brain barrier integrity after traumatic brain injury. Journal of Neuroinflammation. 2023; 20: 244. https://doi.org/10.1186/s12974-023-02923-6.
- [41] Fang M, Yu Q, Ou J, Lou J, Zhu J, Lin Z. The Neuroprotective Mechanisms of PPAR-γ: Inhibition of Microglia-Mediated Neuroinflammation and Oxidative Stress in a Neonatal Mouse Model of Hypoxic-Ischemic White Matter Injury. CNS Neuroscience & Therapeutics. 2024; 30: e70081. https://doi.org/10.1111/cns.70081.
- [42] Decout A, Katz JD, Venkatraman S, Ablasser A. The cGAS-STING pathway as a therapeutic target in inflammatory diseases. Nature Reviews. Immunology. 2021; 21: 548–569. https: //doi.org/10.1038/s41577-021-00524-z.
- [43] Juliet PAR, Mao X, Del Bigio MR. Proinflammatory cytokine production by cultured neonatal rat microglia after exposure to blood products. Brain Research. 2008; 1210: 230–239. https://doi.org/10.1016/j.brainres.2008.02.099.
- [44] Erdei J, Tóth A, Nagy A, Nyakundi BB, Fejes Z, Nagy B, Jr, et al. The Role of Hemoglobin Oxidation Products in Triggering Inflammatory Response Upon Intraventricular Hemorrhage in Premature Infants. Frontiers in Immunology. 2020; 11: 228. ht tps://doi.org/10.3389/fimmu.2020.00228.
- [45] Al Nimer F, Beyeen AD, Lindblom R, Ström M, Aeinehband S, Lidman O, et al. Both MHC and non-MHC genes regulate inflammation and T-cell response after traumatic brain injury. Brain, Behavior, and Immunity. 2011; 25: 981–990. https://doi.org/10.1016/j.bbi.2010.10.017.
- [46] Ren H, Pan Y, Wang D, Hao H, Han R, Qi C, et al. CD22 block-ade modulates microglia activity to suppress neuroinflammation following intracerebral hemorrhage. Pharmacological Research. 2023; 196: 106912. https://doi.org/10.1016/j.phrs.2023.106912.
- [47] Baral H, Kaundal RK. Novel insights into neuroinflammatory mechanisms in traumatic brain injury: Focus on pattern recognition receptors as therapeutic targets. Cytokine & Growth Factor Reviews. 2025; 83: 18–34. https://doi.org/10.1016/j.cytogfr. 2025.03.001.
- [48] Ding R, Li H, Liu Y, Ou W, Zhang X, Chai H, *et al.* Activating cGAS-STING axis contributes to neuroinflammation in CVST mouse model and induces inflammasome activation and microglia pyroptosis. Journal of Neuroinflammation. 2022; 19: 137. https://doi.org/10.1186/s12974-022-02511-0.
- [49] Wu W, Zhang X, Wang S, Li T, Hao Q, Li S, et al. Pharmacological inhibition of the cGAS-STING signaling pathway suppresses microglial M1-polarization in the spinal cord and attenuates neuropathic pain. Neuropharmacology. 2022; 217: 109206. https://doi.org/10.1016/j.neuropharm.2022.109206.

